TABLE 1 Comparisons of the Antenna Size and Bandwidth

Published Literature	Bandwidth Comparison		Antenna Size Comparison (Proposed/Literature) (%)
	LTE700/GSM850/GSM900 Bands (%)	DCS/PCS/UMTS/LTE2500 Bands (%)	
[1] Kuo et al.	889∼974 MHz (9.1)	1668∼1897 MHz (12.8)	17.2
[2] Wang et al.	800∼960 MHz (18.1)	1670∼2120 MHz (23.7)	18
[3] Chi et al	890∼960 MHz (7.6)	1710∼2250 MHz (27.3)	54.3
[4] Wong et al	785∼985 MHz (22.6)	1630∼2300 MHz (34.1)	94.2
[5] Wong et al	820∼990 MHz (18.8)	1700∼2200 MHz (25.6)	90.5
[6] Song et al.	800∼1000 MHz (22.2)	1300∼2670 MHz (69)	38.8
[7] Chiu et al.	880∼960 MHz (8.7)	1700∼2700 MHz (45.5)	64.6
Proposed	659∼973 MHz (38.5)	1689∼2179 MHz (25.3) 2449∼2779 MHz (12.6)	100

change vary significantly. To attain good impedance matching about 698–960 MHz and 1710–2170 MHz, in this study the slot gap is optimized to be $G = 12$ mm.

A parameter study has been performed to evaluate the effects of the strip lengths on return loss. As shown in Figure 4(a), by increasing the length of the L_1 strip, the resonant frequencies in the lower and upper bands decrease. However, the medium bands do not change significantly. The L_2–L_4 strips perform similarly as the L_1 strip to enhance the bandwidths together with the L_1 strip. Figure 4(b) shows that the M_1 strip works for the medium and upper bands but not the lower one. By increasing the M_1 strip length, the resonant frequencies in the upper bands reduce. Likewise, the M_2–M_8 strips function with the M_1 strip to improve the medium and upper bands. For tuning only the upper bands, one may vary the H_1 strip as shown in Figure 4(c). Likewise, the H2 strip radiate in the upper bands too.

A spherical near-field antenna measurement anechoic chamber (NSI) was used to measure antenna radiation properties. Accurate antenna radiation efficiencies and 3D patterns from 500 MHz to 18 GHz can be obtained with this chamber. Figures 5(a)–5(c) exhibit the measured far-field radiation patterns in the *xy*, *yz*, and *xz* planes defined in Figure 1(a) for three frequencies at 800, 1900, and 2600 MHz, respectively. Fairly omnidirectional patterns in those three frequencies are obtained. Also, measured antenna average gains and radiation efficiencies are plotted in Figure 6. For the LTE700 and GSM850/900 bands, the antenna average gain varies from −2.41 to −0.56 dBi and the radiation efficiency is large than 51%, as shown in Figure 6(a). Results in the other bands are given in Figure 6(b). The antenna average gains and radiation efficiencies are from −2.86 to −0.74 dBi and 53–84% for the DCS/PCS/UMTS band and LTE2500 band, respectively. Therefore, good antenna efficiencies are obtained for the LTE700/2500, and WWAN operations with the compact antenna embedded in the ultra-thin laptop computer. In Table 1, comparisons of the proposed antenna with those reported in Refs. 1–7 on antenna dimensions and bandwidths are given. Our antenna is both compact and wideband for suitably integration into the ultra-thin laptop computer.

4. CONCLUSIONS

A compact slot inverted-F antenna for the LTE and WWAN operations has been carefully presented and analyzed. This antenna is flexible in tuning bandwidths and capable of performing good omnidirectional coverage and high radiation efficiencies throughout all the operating bands. Also, compared with previous designs, the proposed antenna with an even more compact size is suitable to be integrated within the u laptop computer as an internal antenna for the LTE700, GSM850/900, DCS/PCS/UMTS, and LTE2500 applications.

REFERENCES

1. C.-H. Kuo, K.-L. Wong, and F.-S. Chang, Internal GSM/DCS dual-band open-loop antenna for laptop application, Microwave Opt Technol Lett 49 (2007), 680–684.
2. X. Wang, W. Chen, and Z. Feng, Multiband antenna with parasitic branches for laptop applications, Electron Lett 43 (2007), 1012–1013.
3. Y.-W. Chi and K.-L. Wong, Compact multiband folded loop chip antenna for small-size mobile phone, IEEE Trans Antennas Propag 56 (2008), 3797–3803.
4. K.-L. Wong and L.-C. Lee, Multiband printed monopole slot antenna for WWAN operation in the laptop computer, IEEE Trans Antennas Propag 57 (2009), 324–330.
5. K.-L. Wong, and F.-H. Chu, Internal planar WWAN laptop computer antenna using monopole slot elements, Microwave Opt Technol Lett 51 (2009), 1274–1279.
6. C.T.P. Song, Z.-H. Hu, J. Kelly, P.S. Hall, and P. Gardner, Wide tunable dual-band reconfigurable antenna, Electron Lett 45 (2009), 1109–1110.
7. C.-W. Chiu and Y-J Chi, Planar hexa-band inverted-F antenna for portable device applications, IEEE Antennas Wirel Propag Lett 8 (2009), 1099–1102.

INDIRECT EVALUATION OF RADIATED EMISSIONS FROM A BENT SIGNAL LINE ON A PRINTED CIRCUIT BOARD WITH TWO ATTACHED CABLES

Dong-yeon Kim,[1] Jae W. Lee,[1] Choon Sik Cho,[1] Haeng S. Lee,[2] and Yeon-Choon Chung[3]

[1] School of Electronics, Telecommunication and Computer Engineering, Korea Aerospace University, 200-1, Hwajeon-dong, Deogyang-gu, Goyang, Gyeonggi-do 412-791, Korea; Corresponding author: jwlee1@kau.ac.kr
[2] Department of Electronic Engineering, Sogang University, 1 Shinsu-dong, Mapo-gu, Seoul, Korea
[3] Department of Information and Communication, Seokyeong University, 16-1, Jungneung-dong, Sungbuk-gu, Seoul 136-704, Korea

Received 19 October 2010

ABSTRACT: *In this article, the radiated emissions mechanism and the variation of radiated emissions level have been analyzed and investigated, respectively, according to the ratio of the horizontal to vertical traces in a bent signal line when a bent signal line on a printed circuit board (PCB) with two attached cables is used. Though many*

papers concerning two cables attached to a PCB have appeared, it is seen that the two cables can be modeled as a dipole antenna. In addition, it is conjectured from two- port S-parameters that the ratio between the horizontal and vertical traces in a bent signal line leads to the variation in magnitude of common-mode voltage induced as a noise source of the dipole antenna. As the signal line in parallel with the attached cable becomes longer, the radiated emissions level due to the current-driven mechanism becomes more dominant while the contribution from the voltage-driven mechanism remains unchanged regardless of the ratio between two signal lines. Based on the analysis of measured and simulated S-parameters, we propose an alternate and relatively simple estimation method replacing the 3-m measuring method to measure the radiated emissions level and investigate the accuracy of our analysis using commercially available software CST MWS 2006B.
 Microwave Opt Technol Lett 53:1832–1837, 2011; View this article online at wileyonlinelibrary.com.
DOI 10.1002/mop.26114

Key words: *attached cables; common-mode; current-drive mechanism; dipole antenna; self-capacitance; voltage-driven mechanism*

1. INTRODUCTION

Recently, the complexity of digital systems has increased with the improvement of system clock frequency and the miniaturization of various electronic devices. These phenomena generate the unintentional possibility for electromagnetic interference (EMI) and electromagnetic emissions between the components, devices, and printed circuit board (PCB) transmission lines. The most important component in radiated emissions from a PCB is widely known as the common-mode current. Although the amount of common-mode current is relatively small compared with that of the differential-mode, it cannot be neglected because of the significant effect it has on the portion of total radiated emissions due to the same direction of current flowing down the signal line and ground plane [1]. Furthermore, it cannot be easily and perfectly removed from the radiation mechanism.

In addition, the inductance induced on the ground plane caused by the common-mode current leads to a voltage drop which is a noise source and cannot provide a stabilized ground voltage. As an example of the maximum radiation due to a common-mode current, we can model electromagnetic radiation from a PCB substrate with attached cables as an equivalent monopole or dipole antenna resulting in the maximum radiation according to the resonant frequency of cable length [2].

In general, the radiation mechanisms resulting from a single trace (transmission line) with attached cables can be categorized into two parts [3]. First, the current-driven mechanism, which induces ground inductance depending on the ground width (W) and the dielectric thickness (h) due to the magnetic field dependent on the time-varying input current, can be modeled by a signal trace terminated with a short circuit [1]. It is well known that the magnitude of the voltage drop formed on the ground plane is proportional to those of the mutual inductance and the time-variant current, and furthermore works as noise source. Second, the effectively induced voltage drop due to the voltage-driven emissions using equivalent an open circuit is proportional to the self-capacitance of the signal trace and driving voltage and is inversely proportional to the self-capacitance determined from the ground size [2].

In this article, the radiated emissions from various bent signal traces according to the ratios of vertical and horizontal line lengths are investigated through a two port circuit implementation and analysis described in Section 2.2 when the cables are attached to the main boards. The effects of horizontal line length relative to vertical line length on the emissions level of the previously categorized mechanisms can be estimated and predicted by evaluating the inductance on the ground and the self-capacitance of signal trace. In addition, the relevant *S*-parameters of an equivalent EMI noise antenna based on modeling the two port network at the signal excitation port and the connector connection port have been investigated, verified, and analyzed through the simulated results based on 3-m radiated emission level measurements.

2. CONFIGURATION AND RADIATION MECHANISM FOR EMI ANALYSIS

Consider the bent signal trace located on the center of a PCB substrate connected with two attached cables as shown in Figure 1. The amount of the common-mode voltage according to the ratios between horizontal and vertical components of the bent signal trace is evaluated by using the substrate information of relative permittivity 2.2 and dielectric thickness (h) 1.5 mm. The width (a) corresponding to the characteristic impedance and the selected ground width for the analysis are 2.9 and 100 mm, respectively. A bent signal trace used for experiment is composed of two traces with horizontal (l_H) and vertical (l_V) maintaining the sum of l_H and l_V equal to 50 mm, respectively.

One volt with constant maximum magnitude at every frequency is inserted at one port, whereas a 50-Ω resistor is connected as a termination at the opposite side. In addition, each length of attached cables is fixed to be 500 mm as an equivalence of extended ground. For this analysis, the discontinuity of the right-angle bend of the single trace has been mitered to minimize the radiation losses and reflection losses.

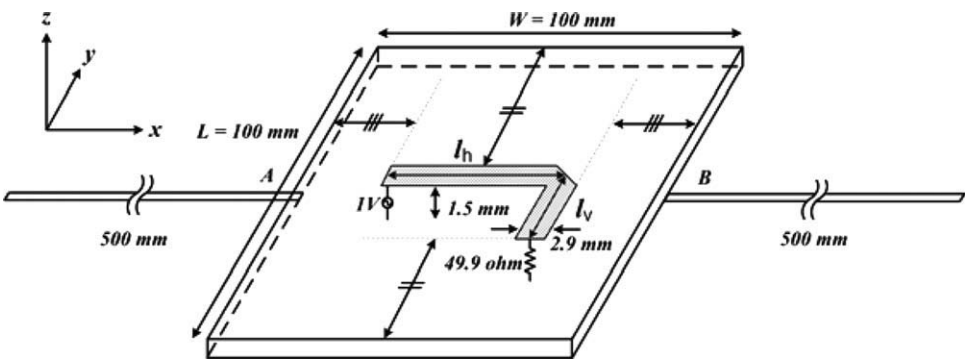

Figure 1 A bent signal trace centered on a PCB substrate with two attached cables [4]

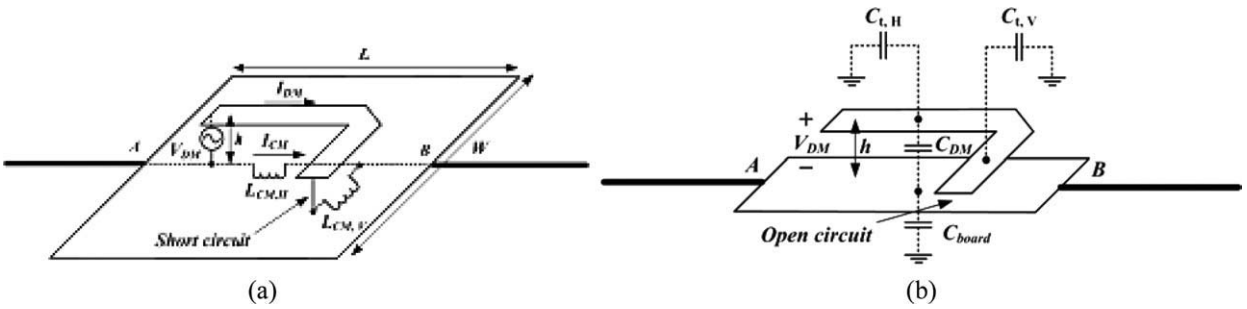

Figure 2 Current- and voltage-driven mechanisms for the PCB structure having a bent microstrip line: (a) current-driven mechanism and (b) voltage-driven mechanism [3]

TABLE 1 The Computed Values of Common-Mode Ground Inductance According to the Ratios of Vertical and Horizontal Traces

	$l_H = 0$ (mm)	$l_H = 10$ (mm)	$l_H = 20$ (mm)	$l_H = 30$ (mm)	$l_H = 40$ (mm)	$l_H = 50$ (mm)
LCM, H	0	0.075	0.15	0.225	0.3	0.375
LCM, V	0.375	0.3	0.225	0.15	0.075	0

$L = W = 100$ mm, $l_H + l_V = 50$ mm, unit: nH.

2.1. Radiation Mechanism from a Bent Signal Line with Attached Cables

Figure 2 describes the two radiation mechanisms from the signal trace terminated with the characteristic impedance on the PCB substrate shown in Figure 1.

2.1.1. Application of the Current-Driven Mechanism. In general, it is well known that the differential-mode currents on vertical and horizontal traces induce ground inductances LCM,H and LCM,V, respectively, denoted by horizontal and vertical inductances in Figure 2(a). It is observed that the current-driven

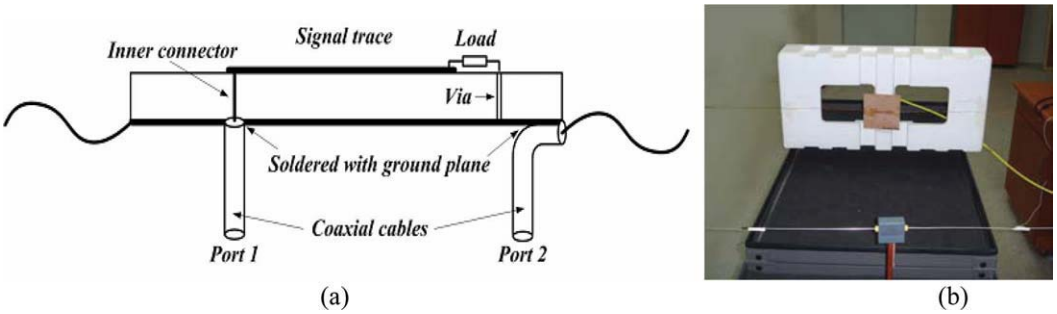

Figure 3 A setup for measuring *S*-parameters for radiated emissions from the PCB with attached cables: (a) cross-section view of the equivalent model and (b) experimental setup. [Color figure can be viewed in the online issue, which is available at wileyonlinelibrary.com]

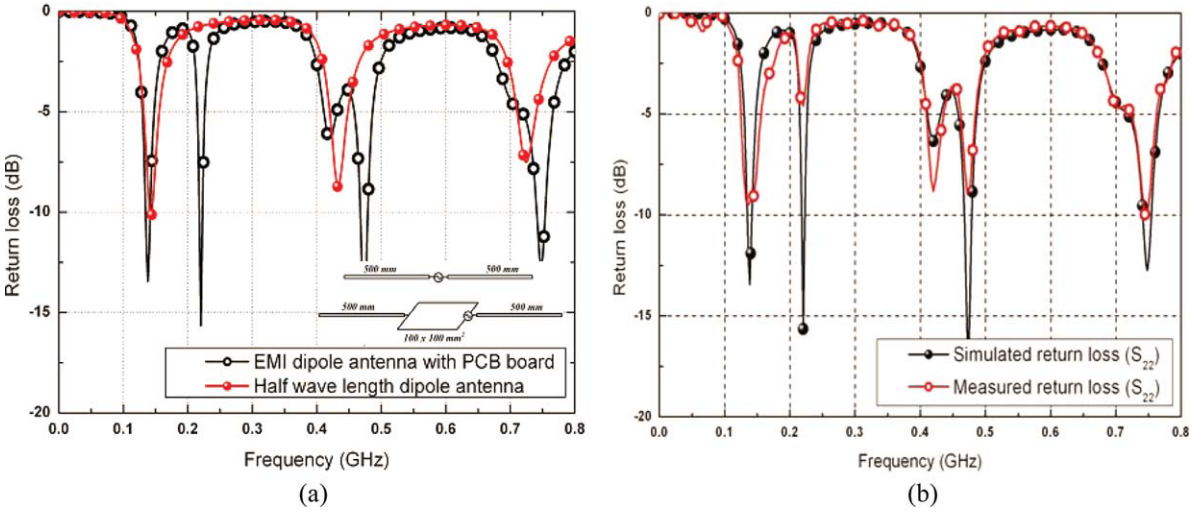

Figure 4 Comparison of simulated return loss characteristics of the EMI dipole antenna attached to the PCB board (a) with that of half wavelength dipole antenna and (b) with the measured data. [Color figure can be viewed in the online issue, which is available at wileyonlinelibrary.com]

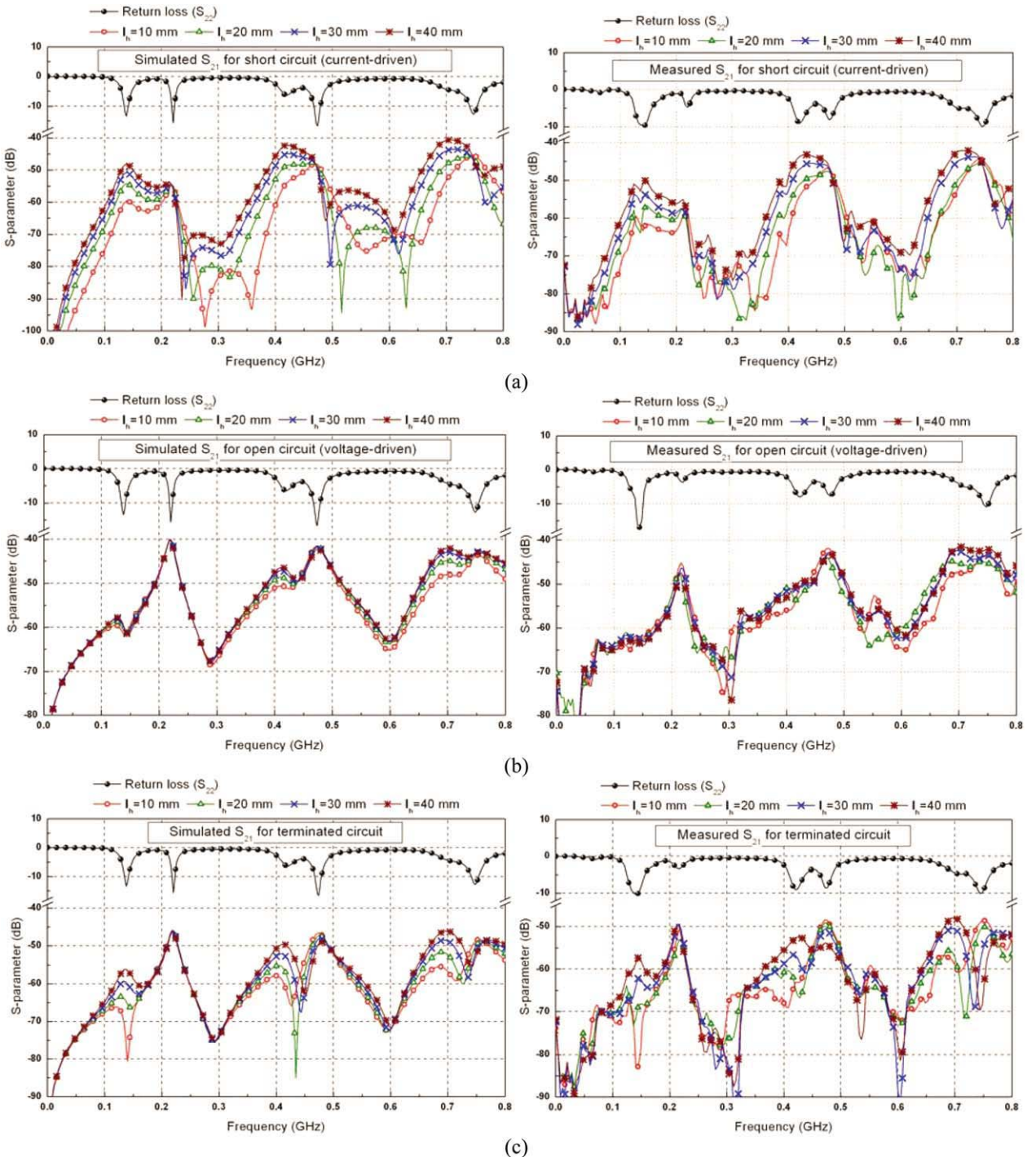

Figure 5 Simulated and measured results (S_{21}) for noise generation according to the ratios between horizontal and vertical traces. [Color figure can be viewed in the online issue, which is available at wileyonlinelibrary.com]

mechanism can be modeled as an equivalent short-circuit and the amount of ground inductance due to the current-driven mechanism is approximated as a function of ground width (W) and dielectric thickness (h) [1]. From Table 1 showing the inductances according to the ratios of horizontal and vertical signal lengths, it is found that the per- length-inductance of each signal trace is 0.075 nH.

Furthermore, it is also claimed that the horizontal (vertical) component of ground inductances increases as the horizontal (vertical) signal trace becomes longer. Hence, the generated inductances on the ground plane induce the voltage drop and determine the magnitude of the EMI noise source. Especially, the voltage drop between contact points A and B in the proposed structure of Figure 2(a) is mainly dependent on the inductance LCM,H induced by the horizontal signal trace. It is also assumed through this article that the increase of ground inductance due to edge effects can be neglected [3].

2.1.2. Application of the Voltage-Driven Mechanism. The equivalent circuits of the voltage-driven mechanism for a bent transmission line and attached cables can be represented as shown in Figure 2(b) using open circuits. It is generally known

that the radiated emissions level due to the voltage-driven mechanism is determined from the magnitude of the self-capacitance and its magnitude depends on the ground size (W), dielectric thickness (h), signal width (a), and per-unit-length self-capacitance [2, 5].

In the case of a bent transmission line with attached cables as proposed in this article, the total self-capacitance can be estimated from the summation of two self-capacitances (due to vertical trace (Ct,V) and horizontal trace (Ct,H) in parallel). Using the given data in this article, we can obtain a total self-capacitance equal to 3.44 [10^{-14} F] derived by $0.0688\times$ ($l_H + l_V$). The voltage drop caused by the voltage-driven mechanism is proportional to the amount of the self-capacitance. In other words, the magnitude of voltage drop due to the voltage-driven mechanism is determined from the total signal length irrespective of the ratios of vertical and horizontal signal traces. Hence, it is conjectured that there are no change in the radiated emissions level and the *S*-parameter values due to the voltage-driven mechanism because of the constant total length.

2.2. Two-Port Circuit Implementation and Analysis

Figure 3 describes the simplified measurement setup for *S*-parameters of the equivalent EMI noise dipole antenna. Using the simplified equivalent measurement setup consisting of Port 1 and Port 2 where the inner and outer conductors of Port 1 are connected with the signal line and ground, respectively, as a source and Port 2 is modeled as an EMI antenna noise source caused by the PCB signal line. The magnitude (S_{21}) of the EMI noise source is investigated according to the load conditions describing radiation mechanisms.

2.2.1. EMI Radiation from the Dipole Antenna. To theoretically investigate the resonant frequencies caused by the PCB board with attached cables, the return loss characteristics of the half wavelength dipole without the PCB and modeled EMI dipole antenna with the PCB board have been suggested for comparison with the measured data in Figure 4. From the simulated data in Figure 4(a), it is seen that dipole antenna composed of each physical length of 500 mm generates a fundamental resonance at the frequency corresponding to the electrical length $\lambda/2$ and the resonances occur at 142, 433, and 725 MHz, respectively. On the other hand, EMI dipole antenna with PCB board generates additional resonances near the frequencies of 218 MHz due to the asymmetrical effect in antenna geometry. This means that the EMI components inevitably existing inside PCB can be effectively and easily radiated into the free space at the neighborhood of the resonance frequencies. In addition, it is conjectured from Figure 4(b) that the simulated and measured results show good agreement.

2.2.2. EMI Phenomenon Due to Attached Cables. From the measurement setup for the *S*-parameters shown in Figure 3, the variation and trend of EMI-radiated emissions generated from the PCB attached with two cables are evaluated and predicted as a function of load condition. Furthermore, the resonant frequencies of the EMI noise dipole antenna according to the cable lengths are estimated through the return loss (S_{22}) at Port 2. It is found that the characteristics of return loss remain unchanged irrespective of load condition. Figure 5(a) describes the variations of S_{21} related with the current-driven mechanism modeled by a short circuit at the load. As a result, it is seen that the coupling effects caused by the current-driven mechanism become smaller as the horizontal length of the signal line decreases. In addition, Figure 5(b) delineates the variations of S_{21} related with

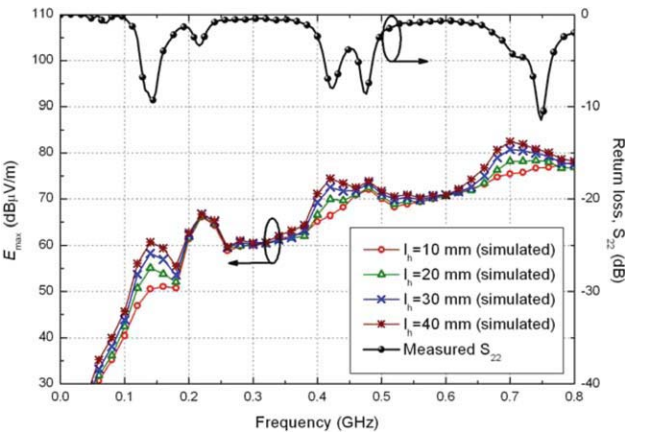

Figure 6 The estimated variations of radiated emissions level according to the ratios between horizontal and vertical traces. [Color figure can be viewed in the online issue, which is available at wileyonlinelibrary.com]

voltage-driven mechanism governing the open circuit as a load condition. It is also observed from Figure 5(b) that the shape of the return loss does not change irrespective of the ratios of horizontal and vertical signal lengths. Likewise, the results shown in Figure 5(c) demonstrate that when the signal line is matched at 50 Ω, the transmission effects at the frequencies, 140, 420, and 700 MHz governed by the current-driven mechanism become considerably smaller, implying that the magnitude of the EMI antenna noise source decreases, as the horizontal component (l_H) of signal line decreases. However, the variation of S_{21} at the frequencies, 220, 470, and 740 MHz controlled by the voltage-driven mechanism is relatively weak, indicating that the EMI antenna noise source is constant.

3. CIRCUIT IMPLEMENTATION AND PERFORMANCE EVALUATION

Above, it is verified that the amount of noise generated by the equivalent EMI-modeled dipole antenna according to the relative ratios between horizontal and vertical signal traces is mainly dependent on the increase of the horizontal component through the measured and simulated S_{21} described in Section 2. As comparison data, Figure 6 depicts the simulated radiated emissions level using the 3-m measurement method from a few megahertz to 800 MHz. It is conjectured from Figure 6 that as the horizontal component increases from 10 to 40 mm, the current-driven mechanism is more dominant and leads to the important role in the resonant frequencies of odd number, while the radiated emissions mainly governed by the voltage-driven mechanism result in the resonant frequencies of even number and do not change. The variation in S_{21} at 138, 422, 708 MHz governed by the current-driven mechanism as shown in Figure 5(a) is within 9 to 13 dB. As expected, the variation range is almost equal to the variation of the radiation level simulated at the same frequencies in Figure 6.

In other words, by using the *S*-parameter measurement setup modeled and depicted in Section 2, we can indirectly estimate and predict the resonant frequency of maximum radiated emissions and the variation amount of radiated emissions according to the ratios between horizontal and vertical components comprising a bent signal trace.

4. CONCLUSIONS

In this article, as a simple and practical method for measuring the variation of radiated emissions of signal traces, *S*-parameters

measurement according to the ratios of the horizontal component relative to the vertical trace has been investigated by considering the common-mode radiated emissions from a PCB substrate with a bent signal trace and attached cables. In addition, in order to analyze the radiation mechanism, it is shown that the PCB substrate connected with attached cables could operate as an EMI dipole antenna by simulating and measuring the resonant frequency. As a result, in the case where the total signal length is kept constant, it is ensured from the results that as the horizontal signal line in parallel with attached cables becomes longer, the radiated emissions level due to the current-driven mechanism increases while there is no variation in the radiated emissions level due to the voltage-driven mechanism. In particular, as an advantage of this method, it is guaranteed that the conventional 3-m measuring method to estimate the radiated emissions can be replaced by an implementation of a simple two-port network and measuring the trend of variation in radiated emissions and resonant frequencies.

REFERENCES

1. C.R. Paul, A comparison of the contributions of common-mode and differential-mode currents in radiated emissions, IEEE Trans Electromagn Compat 31 (1989), 189–193.
2. D.M. Hockanson, J.L. Drewniak, T.H. Hubing, and T.P. Van Doren, FDTD modeling of common-mode radiation from cables, IEEE Trans Electromagn Compat 38 (1996), 376–387.
3. D.M. Hockanson, J.L. Drewniak, T.H. Hubing, T.P. Van Doren, F. Sha, and M.J. Wilhelm, Investigation of fundamental EMI source mechanisms driving common-mode radiation from printed circuit boards with attached cables, IEEE Trans Electromagn Compat 38 (1996) 557–566.
4. D.-Y. Kim, J.W. Lee, C.S. Cho, and Y.-C. Chung, Alternative investigation of common- mode radiated emission from PCB with a bent signal line and attached cables, Proceedings of Asia-Pacific Microwave Conference (APMC), Bangkok, Thailand, Dec. 15–20, 2007.
5. D.M. Hockanson, J.L. Drewniak, T.H. Hubing, T.P. Van Doren, F. Sha, C.W. Lam, and L. Rubin, Quantifying EMI resulting from finite-impedance reference plane, IEEE Trans Electromagn Compat 39 (1997), 286–297.
6. H.W. Shim and T.H. Hubing, Model for estimating radiated emissions from a printed circuit board with attached cables due to voltage-driven sources, IEEE Trans Electromagn Compat 47 (2005), 899–907.
7. H.W. Shim and T.H. Hubing, Derivation of a closed-form approximate expression for the self-capacitance of a printed circuit board trace, IEEE Trans Electromagn Compat 47 (2005), 1004–1008.

A NOVEL PRINTED MONOPOLE ANTENNA FOR FUTURE ULTRA-WIDEBAND COMMUNICATION SYSTEMS

Osama M. H. Ahmed and Abdel-Razik Sebak
Department of Electrical and Computer Engineering, Concordia University, 1455 de Maisonneuve West, Montreal, Quebec H3G 1M8, Canada; Corresponding author: o_ahm@encs.concordia.ca

Received 19 October 2010

ABSTRACT: *In this letter, a novel microstrip line-fed printed monopole antenna for ultra-wideband (UWB) short-range wireless communications is proposed. The proposed antenna consists of a trapezoidal-shaped patch with two elliptical-shaped cuts from its edge forming a bell-shaped cut. Experimental results shows that the designed antenna operates over impedance bandwidth 3.2–11.4 GHz for return loss* $S_{11} < -10$ *dB, which almost covering the UWB frequency bandwidth. Moreover, the antenna has a good omnidirectional radiation patterns in the* H*-plane with good gain flatness over the frequency range of interest. The antenna transmission characteristics at different receiving angles are also measured. By embedding a simple narrow U-shaped slot in the radiating microstrip patch, a notch in the frequency band of 5.0–6.0 GHz is obtained. The proposed antenna is considered a good candidate for UWB short-range wireless communication systems avoiding the interference of the existing wireless systems.* © 2011 Wiley Periodicals, Inc. Microwave Opt Technol Lett 53:1837–1841, 2011; View this article online at wileyonlinelibrary.com. DOI 10.1002/mop.26113

Key words: *ultra-wideband; printed monopole antennas; trapezoidal antennas; compact antennas, band-notched antennas*

1. INTRODUCTION

Because of rapid development in ultra-wideband (UWB) systems in recent years, antennas with absolute frequency bandwidth of up to 7.5 GHz (or fractional bandwidth of up to 110%) operating from 3.1–10.6 GHz frequency spectrum become demanding in practical applications for short-range wireless communications. Many antenna parameters can affect the design procedure such as antenna bandwidth, radiation pattern, size, and manufacturing technology. Several UWB antennas have been introduced such as slot antenna [1], Vivaldi antenna [2], biconical antenna [3], log-periodic antenna, spiral antenna [4], and printed monopole antenna [5, 6]. Because of their simple design and omnidirectional radiation pattern, printed monopole antennas are considered one of the most popular antennas in UWB systems.

In recent years, a noticeable interest in antenna design for UWB technology with a single band-notch function in the 5.0–6.0 GHz frequency band has been increased. This is to avoid interferences with the other existing wireless local network (WLAN) systems working in the same UWB frequency band, that is, 5.15 and 5.825 GHz for IEEE 802.11a or HIPERLAN/2. Several techniques have been used to achieve a single band notch within this frequency band. One technique is achieved by

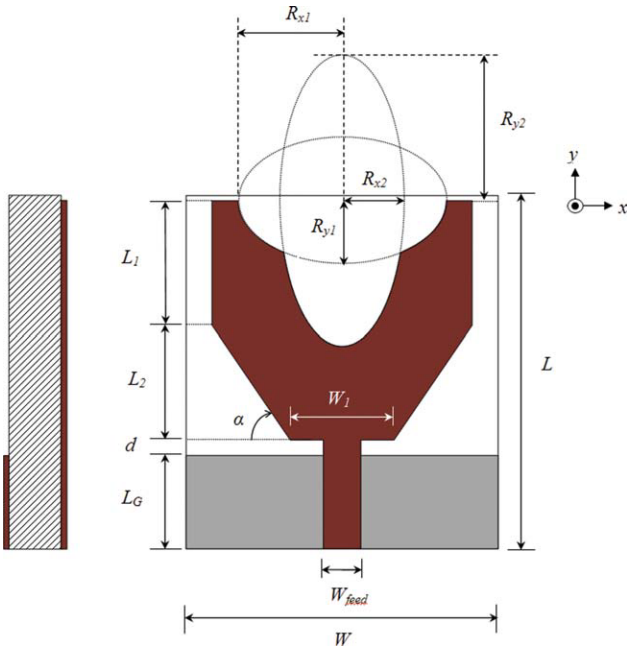

Figure 1 Geometry of the proposed UWB antenna design: top and side view. [Color figure can be viewed in the online issue, which is available at wileyonlinelibrary.com]